Oceanologia, corrected, in press
Polish Academy of Sciences
Institute of Oceanology
Open access article under the CC BY license
https://doi.org/10.5697/EQPL2437

Estimates of the typical wave approach angle from wave-induced water velocity directions in the nearshore of the Gulf of Riga, eastern Baltic Sea

Tarmo Soomere[1,2,*], Maris Eelsalu[1], Kevin Parnell[1], Laura Piho[3]

Abstract
The intensity of coastal processes and particularly wave-driven sediment transport crucially depends on the approach angle of wind waves to the shore. While this angle is usually only a few degrees on the open ocean shore, it is often much larger on the shores of smaller water bodies. We present results of an experiment in the nearshore of the Gulf of Riga, eastern Baltic Sea, over 5 weeks in August–September 2022 using one Acoustic Doppler Velocity (ADV) recorder and nine hydromasts mounted on a rigid frame of 20×20 m and deployed about 400 m from the shore at a depth of about 4 m. Waves that generated near-bottom velocities ≥ 0.15 m/s approached this location mostly from west-north-west, from a narrow range of directions from 270° to 320° clockwise from the North. They typically approach the shore at an angle of $30° \pm 15°$ with respect to the shore normal and generate much stronger alongshore transport than waves with the same height and period but approaching at smaller angles. We also demonstrate that hydromasts are suitable for the recording of wave directions.

Keywords
Baltic Sea; Wind waves; ADV measurements; Hydromasts; Wave direction

[1] *Department of Cybernetics, School of Science, Tallinn University of Technology, Ehitajate tee 5, 19086 Tallinn, Estonia*
[2] *Estonian Academy of Sciences, Kohtu 6, 10130 Tallinn, Estonia*
[3] *Centre for Biorobotics, School of Information Technologies, Tallinn University of Technology, Akadeemia tee 15A, 12618 Tallinn, Estonia*
***Correspondence**: tarmo.soomere@taltech.ee (T. Soomere)

Received: 23 December 2025; **revised:** 9 July 2026; **accepted**: 13 July 2026

1. Introduction

The evolution of sedimentary shores crucially depends on several properties of waves that approach these shores (Carter, 2002). It is customary to attribute the course of coastal processes, more generally, the development of the shore, to the orientation of the shoreline, properties of waves, particularly the prevailing storm wave direction (Kilar et al., 2025), the morphology of the nearshore (shoreface slope, presence or absence of bars), and water-level fluctuations. However, this course substantially depends on all three core properties of wave fields – wave height, period and direction. The dependence on wave height and direction is explicit. The intensity of wave-driven alongshore sediment transport has been shown to be proportional to the approaching wave height H to the power of at least 2 (Kamphuis, 1991; USACE, 2002). Therefore, an increase in the wave height by 10% would lead to intensification of transport by at least 21%. Transport intensity has also been shown to depend on the approach angle θ, that is, the angle between the wave propagation direction and shore normal. The transport has been shown to be proportional to $\sin 2\theta$ (USACE, 2002) or even $\sin^{0.6}(2\theta)$ (Kamphuis, 1991). This property underlines the role of the wind and wave direction for coastal processes. In particular, it implies that even a seemingly minor uncertainty in the specification of the wave approach direction may lead to significant over- or underestimation of the intensity of wave-driven alongshore transport. The particular values of wave period usually have a smaller impact on this transport. The wave period enters only into the direction-dependent expression for the CERC (Coastal Engineering Research Council) coefficient where one of the terms contains the maximum orbital velocity at the breaker line (USACE, 2002) while the Kamphuis (1991) formula contains the peak wave period to the power of 1.5. However, shoaling and refraction, both of which depend on wave period may significantly influence the magnitude of wave-driven transport. These processes may considerably redirect the wave field and increase the wave height and

© 2026 The Author(s). This is the Open Access article distributed under the terms of the Creative Commons Attribution Licence.

thus also properties of breaking and the location of the breaker line.

The strong dependence of wave-driven transport on the wave approach angle is among the main reasons why about 50% of the world's coastline is at risk from wave climate change (Morim et al., 2019). This is also one of the reasons why storms with anomalous wave directions may cause severe coastal erosion (Harley et al., 2017; Mortlock et al., 2017) in many locations. The impact of waves on the coast may drastically change even when the approach direction of storm waves varies (or is misinterpreted) as little as 5° compared to the usual direction (Flor-Blanco et al., 2021). Thus, adequate specification of the wave approach direction is critical for quantification of wave-driven impact on seabed and sediment transport. Even small inaccuracies in the estimation of wave approach directions may lead to larger predicted impacts than, for example, sea level rise (Pereira and Coelho, 2013), and may have comparable effect to that of wave height change (Rajasree and Deo, 2018).

The increase in wave heights has been moderate even under rapid climate change in the World Ocean (Young et al., 2011; Young and Ribal, 2019; Timmermans et al., 2020). There has been almost no increase in wave heights in some basins, such as the Baltic Sea (Sokolov and Chubarenko, 2024). On the contrary, major changes in the wind directions (Bierstedt et al., 2015), directions of air flow and associated properties of potential sediment transport along the eastern Baltic Sea shores (Soomere et al., 2015) and directional structure of wave energy flux (Eelsalu et al., 2024) have occurred in the Baltic Sea basin.

More generally, on many occasions, mean wave direction is the metric most closely linked to changes in the shoreline (Xu et al., 2024). Zacharioudaki and Reeve (2011) even conclude that "material shoreline changes are generally linked to significant changes in future wave direction rather than wave height". Even subtle changes in wave direction have been found responsible for the reversal in the net alongshore sediment transport direction and opposing patterns of morphology change (Stevens et al., 2024). The associated changes to wave properties substantially depend on the seabed morphology that is commonly fairly complex in the Baltic Sea. The related effects are often the strongest for shorelines whose orientation extensively varies (Sanuy and Jiménez, 2019) and in areas where an increase in the wave energy flux is combined with a rotation of wave approach direction (Ghanavati et al., 2024).

Changes to the prevailing wave approach direction seem to be an intrinsic feature of the long-term course of wave properties in many areas of the World Ocean over millennia (Silva et al., 2020). Seasonal variations in the predominant wave direction in a bi-directional wave climate (Wiggins et al., 2019; Elshinnawy and Antolínez, 2023) and associated variations of impacted beaches (e.g., Dolphin et al., 2011) are characteristic of many regions, such as the Yellow Sea and the East China Sea (Woo et al., 2023), the Bohai Sea (Ren et al., 2017) or Indonesia (Wiguna and Dompeipen, 2025). Multi-annual variations often occur in regions impacted by large-scale weather patterns, such as El Niño (McSweeney, 2020) or the North Atlantic Oscillation (Thomas et al., 2011), Pacific-South American modes (Echevarria et al., 2020) or the Pacific Decadal Oscillation (Stevens et al., 2024). Systematic changes in wave propagation or approach direction, attributable to climate changes, have been identified in many regions of the World Ocean, both in different parts of the open ocean (Chile, Gómez et al., 2024; Arctic Ocean, Casas-Prat and Wang, 2020; Bay of Biscay, Charles et al., 2012a,b) and in inland seas, such as the Mediterranean Sea (Casas-Prat and Sierra, 2010). The most pronounced changes over the last 140 years – an anticlockwise rotation in wave direction of up 5° – have been projected for the Southern Hemisphere (Hemer et al., 2010; Meucci et al., 2023).

The examples presented above call for enhanced attention to the analysis of wave directions in the nearshore. While the direction of regular swells can be easily determined, the specification of the wave propagation direction for wind-seas is a challenge (Mi et al., 2025). Wave direction is customarily evaluated from spectral models or from directional waveriders. There are very few attempts to directly quantify wave approach directions in the nearshore in locations where wave properties are not necessarily properly resolved by contemporary wave models. It is traditional to apply various approximations to evaluate the wave propagation direction at the breaker line (that is used in the CERC formula for wave-driven transport) from the modelled or measured data at some distance from the shoreline (Larson et al., 2010; Soomere et al., 2013).

In this paper we describe the results of direct measurements of directions of wave-driven near-bottom velocities. These directions are interpreted as wave propagation directions based on the understanding that water velocities in surface waves are collinear with the wave propagation direction. We employ for this purpose high-resolution measurements of near-bottom velocities in the nearshore of the eastern shore of the Gulf of Riga. The main features of this experiment and an analysis of non-directional properties of near-bottom velocities are provided by Eelsalu et al. (2025). The focus is on directional properties of waves that provide most of the wave energy flux in this location.

Our goal is to physically measure wave approach directions in the nearshore in a location where wave properties are only roughly reflected by wave models but where waves are not yet breaking. This task is solved by means of accurately measuring the direction of wave-driven near-bed water velocities. As we are specifically interested in quantification of the approach direction of waves of appreciable height (that produce most of alongshore sediment transport), we use for this purpose one Acoustic Doppler Velocimeter (ADV) and an array of nine hydromasts. These

In Press

devices have been developed for hydrological applications, primarily for continuous measurements of flow properties (Ristolainen et al., 2016, 2019; Egerer et al., 2024). These and similar instruments are also used in marine wave-dominated oscillatory conditions to evaluate properties of relatively intense water flows, with the main goal to quantify the properties of distributions of large water speeds (Eelsalu et al., 2025).

The paper is structured as follows. We start from a description of the study area, the experimental site, the configuration and set-up of the campaign, the deployed devices, and data preprocessing procedures. This information is complemented with local hydrometeorological conditions at the study site, including properties of incoming wave fields recorded by a nearby surface device and simulated using a multi-nested SWAN wave model during the experiment and in 1990–2022, in Section 2. Section 3 provides an insight into probability density distributions of directions of water motions recorded by different devices and provides a comparison of the outcome from different recordings. The main results are formulated in Section 4.

2. Study area, experiment set-up, recording devices and data preprocessing

2.1 Location

To quantify the typical wave approach direction in the immediate vicinity of the surf zone, a dedicated experiment was conducted near the Port of Skulte in the south-eastern nearshore of the Gulf of Riga (Figure 1). This semi-sheltered water body with an oval-like shape in the eastern Baltic Sea has dimensions of approximately 130×140 km, a surface area of 17,913 km^2, and average and maximum depths of 26 m and 66 m, respectively (Stiebrins and Väling, 1996; Skudra and Lips, 2017). The largest single notable features are the island of Ruhnu and an area of seabed elevation, Gretagrund, near the geometric centre of the gulf. The bathymetry is generally regular: the isobaths down to about 20 m are mostly parallel to the shore and the bottom of the deeper part is largely even. Only the northern and north-eastern (NE) parts of the gulf have numerous small bays, islands and islets, and there is the >60 m deep Mersrags Trench in the south-west (SW) of the gulf (Tsyrulnikov et al., 2008). These features are located >50 km from the experiment site.

The experiment site is open to the two most frequent directions of moderate and strong winds in the region: SW and north-north-western (NNW) winds (Soomere, 2003; Eelsalu and Soomere, 2026). Waves excited by these winds are responsible for most of the wave-driven sediment transport along the entire eastern shore of the Gulf of Riga (Eelsalu et al., 2024; Soomere et al., 2025). It is thus likely that the experiment site adequately reflects the typical wave conditions that contribute to the alongshore sediment transport and that waves in the nearshore of this site reflect well wave properties that exist farther offshore.

Measurements of near-bottom velocities were performed about 500 m from the shore in about 4 m deep water. This location at 57°19′16.6′′N, 24°23′33.8′′E (Figure 1) was located near the seaward end of a gently sloping nearshore area. The closure depth (down to which wind waves effectively shape the coastal profile) is about 4.5 m in this area (Soomere et al., 2017). As wave heights were relatively modest during the experiment (see below), waves were generally not yet breaking at the measurement site. As mentioned above, isobaths down to the depth of about 20 m were generally parallel to the shoreline. The 10 m isobath was located approximately 2 km from the shore (1.5 km from the experiment site). It is therefore likely that wave refraction occurred more or less homogeneously along the shoreline and thus the wave properties at any point of the nearshore directly reflect the offshore wave parameters, with possible modifications via refraction and shoaling in a plane geometry. As the average of both velocity components recorded by the ADV over the entire duration of the experiment was very small (-0.0030 m/s and 0.0028 m/s; Eelsalu et al., 2025), it is likely that the recorded velocities were mostly wave-driven.

2.2 Devices

The experiment was performed in this location over a period of about five weeks from 2 August to 8 September 2022. As detailed properties of the devices used, the measurement routine, the data sets and the data preprocessing are provided by Eelsalu et al. (2025), we refer to that source for more detailed information than is presented here. Two types of devices were mounted to the seabed and employed to measure near-bottom velocities in a slightly different manner. We use the notion “velocity” for the velocity vector and “speed” for the associated scalar property.

Nine hydromasts (Ristolainen et al., 2016, 2019) were mounted at a distance of 10 m from each other on a rigid aluminium frame with the dimensions of 20×20 m (Figure 2). The average water depth at the location of devices (referred to as H01–H09) varied from 4.03 to 4.064 m. An ADV (Nortek Vector) was mounted at the centre of this configuration adjacent to H05 (Figure 2). The raw data was stored locally in the devices for the entire experiment period.

Hydromasts are designed to measure flow speed in the range of 0.15–1.0 m/s and flow direction with an accuracy better than 10° (Egerer et al., 2024). However, the analysis by Eelsalu et al. (2025) showed that the devices provided reliable recordings starting from about 0.11–0.12 m/s. Even though the flow direction may be reliably recorded at even lower flow speeds, we only use the data that correspond to flow speeds above the thresholds of reliability for each device as presented in Eelsalu et al. (2025). The hydromasts recorded pressure fluctuations and a proxy of water speed

In Press

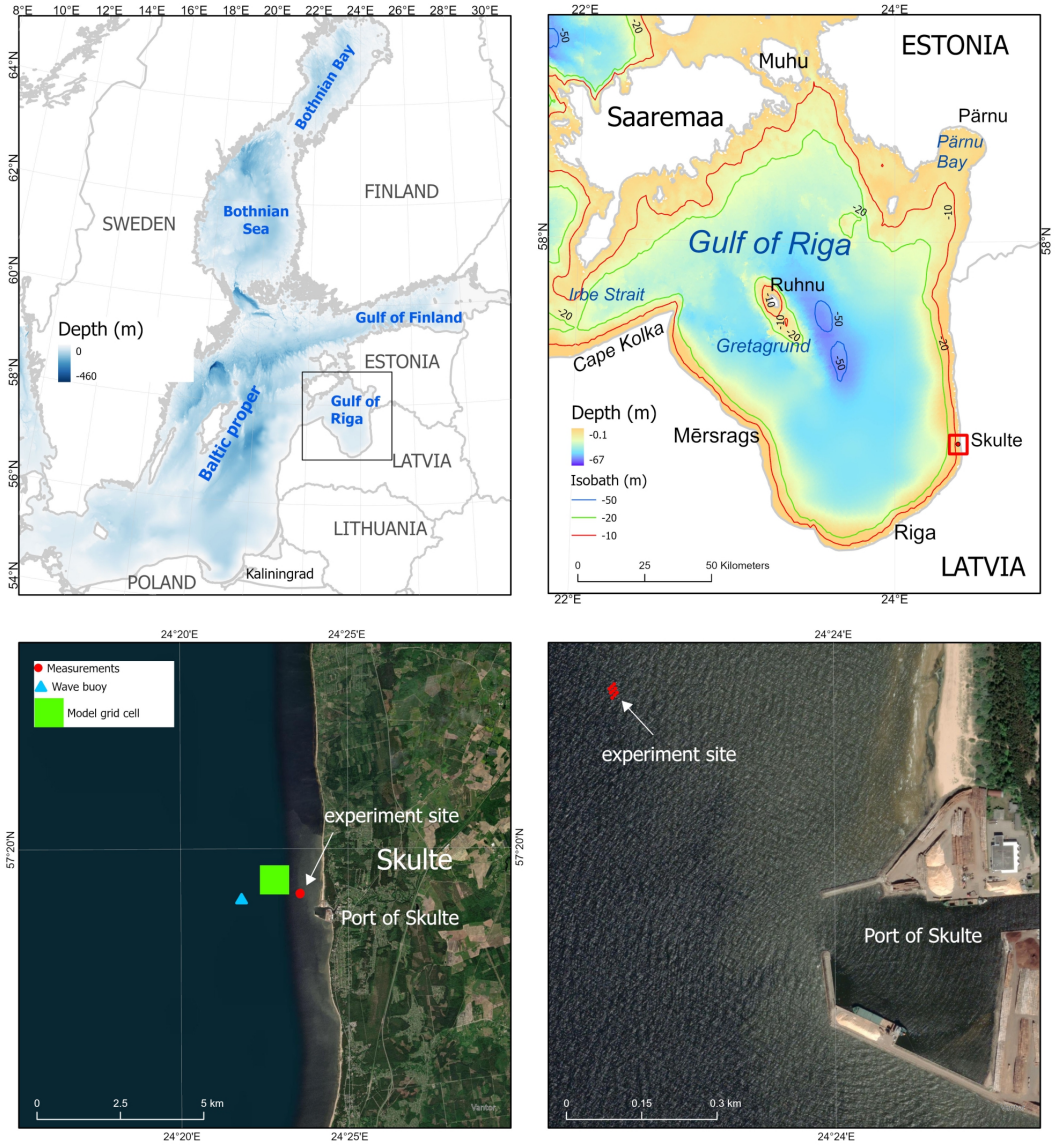


Figure 1. Location scheme of the Gulf of Riga in the eastern Baltic Sea (upper panels) and schematic of the experiment site, location of the wave buoy, the closest grid cell of the SWAN wave model and configuration of the Port of Skulte (lower panels).

and direction continuously during the entire experiment period at the rate of 50 Hz. The directional resolution was 1°. The devices were equipped with a real time clock, an absolute pressure sensor, a polycarbonate hollow vibrating mast and a Hall sensor for the detection of flow speed and direction, and an onboard compass for orientation. The measuring points of water velocity and pressure were at the height of 0.45 m and 0.05 m, respectively, above the seabed.

The ADV recorded all three velocity components at 8 Hz. Its sampling volume was approximately 0.4 m above the seabed, that is, almost equal to the measurement points of the hydromasts. The data were sampled in two-minute bursts (960 samples) every half hour during the entire experiment. The devices were deployed on 2 August and retrieved on 8 September 2022. In the analysis below we use the data from full days 3 August to 6 September.

2.3 Preprocessing

The internal clocks of the hydromasts developed differences of a few seconds over six weeks from their set-up until the data was read. As we are interested in statistical properties of wave propagation directions, these differences are immaterial for the analysis below. However, the time stamps of the devices were aligned using an electromagnetic synchronisation coil before and after the deployment.

The proxy data of velocities recorded by the hydro-

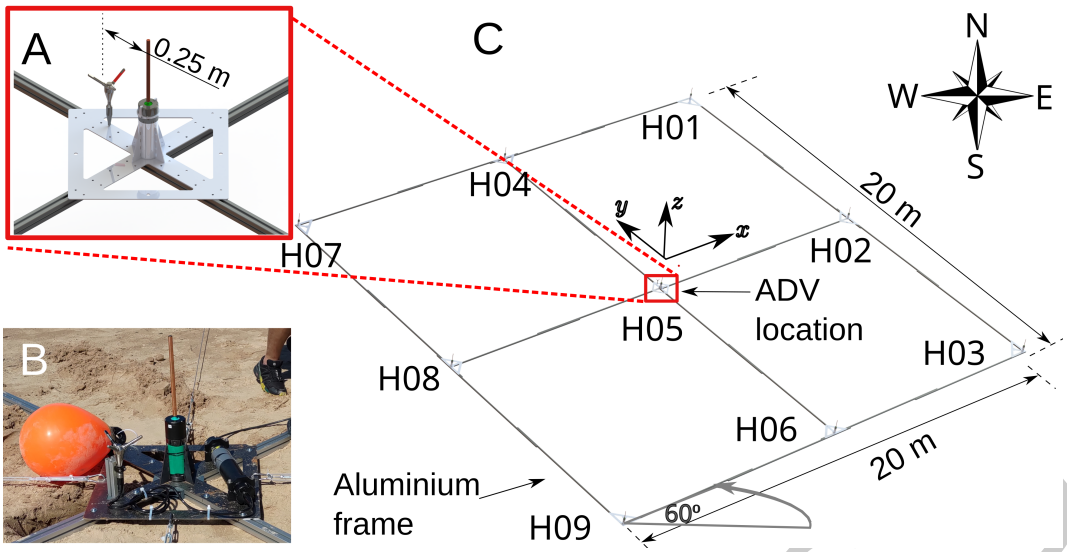


Figure 2. Schematic of mounting of the devices (A, B) and orientation of the frame (C). The orientation of the frame from H07 to H01, H08 to H02 and H09 to H03 is 60° to the east of the direction to the North. The small system of coordinate axes near H05 reflects the orientation of the ADV coordinate system. Amended from Eelsalu et al. (2025) by Laura Piho.

masts were converted into physical units using the procedure described in Egerer et al. (2024). The data were filtered using a median filter that removes spurious peaks. The relevant analysis is provided by Eelsalu et al. (2025). The hydromasts are designed to reliably record velocities from 0.15 m/s (Ristolainen et al., 2016, 2019; Egerer et al., 2024). This threshold was exceeded only in about 5% of single recordings at this experiment site (Eelsalu et al., 2025). However, the output of the hydromasts in terms of velocity was adequate starting from water speeds of 0.1025–0.1175 m/s (Eelsalu et al., 2025). The share of velocities that are detected reliably is about 10% of the entire pool of recordings (Eelsalu et al., 2025). It is likely that the range of reliability of the detection of flow direction is even wider; however, we limit our analysis to these thresholds.

The recordings of directions of water motion were converted into physical directions using simple rotation based on the readings of the internal compass devices. Following the standard notion in wave measurement and modelling, these directions showed to where water was flowing. Directions were recorded anticlockwise in degrees from the east (0°) in both the positive direction to the North (90°) and then to the west until 180° and in the negative direction to the south (−90°) and to the west until −180° (Figure 3). Hydromast H03 recorded directions from the west, and this was corrected in the preprocessing stage. The recordings contained a small number (less than 0.01%) of invalid entries (replaced by NaN, not-a-number, in the retrieved time series) of velocity, direction, or both. These entries are ignored in the analysis. The valid recordings of directions were converted to the standard hydrometeorological frame (degrees clockwise from the North (0°)) via a linear transformation.

The ADV data (1826 bursts in total) were first visually checked for spurious data spikes. Four early bursts and the last 46 bursts, representing the time before deployment and after recovery, were discarded. Also, five bursts that contain a high velocity peak ∼1 m/s on the background of motions ∼0.05 m/s were also excluded from the analysis. The analysis of water velocities, their variability and intermittency (Eelsalu et al., 2025) in the remaining 1771 bursts revealed that the background current was very weak, empirical distributions of velocity components and water speeds generally followed an exponential (rather than Rayleigh or Forristall) distribution, and that speed recordings by hydromasts were reliable to some extent beyond their validated measurement range (Eelsalu et al., 2025).

The ADV device produced output of flow components in the right-hand (x, y, z) coordinates. The probe was oriented so that the x-axis was directed at 60° clockwise to the East from the magnetic North direction. Magnetic declination (the angle between magnetic North and true North) in Skulte, Latvia, around August 2023, was approximately +7.5° east (meaning that magnetic North is 7.5° east of true North). Therefore, the x-axis of the probe was directed at 52.5° to the east from true North (Figure 2).

The recordings of flow velocity components were first converted into the West-East (u) and South-North (v) velocity components using a simple rotation. The x-axis in this coordinate frame was directed to the true East and the y-axis to the true North. The directions of water velocity were calculated in degrees. As with the hydromast data, we used the standard notion of meteorology that assigns zero direction to the North and counts directions clockwise. The shoreline is oriented almost exactly in the

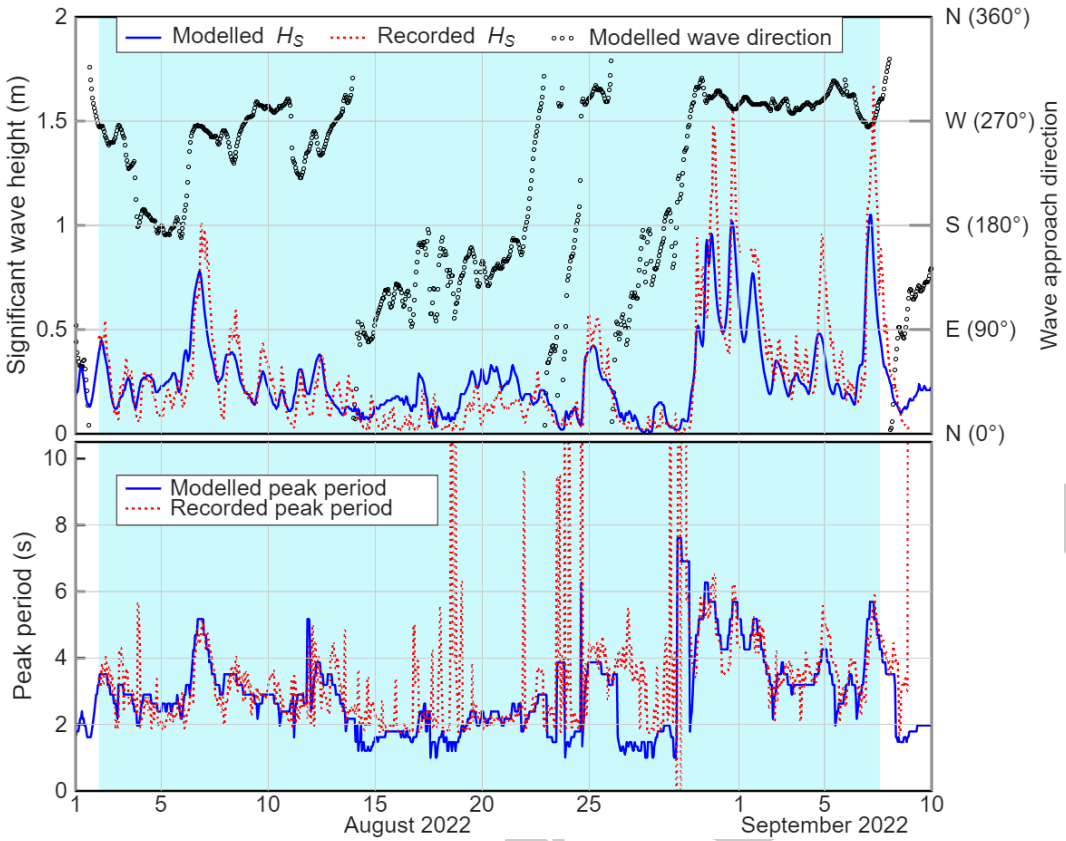


Figure 3. Recorded and modelled significant wave height and peak period, and modelled wave approach direction in the vicinity of the experiment site during the field campaign (light blue shading) in 2022.

South-North direction, that is, in the direction from 180° to 0°/360° and the direction to the East (90°) is the landward direction of shore normal.

2.4 Hydrometeorological conditions

As the local hydrometeorological conditions during the experiment have been discussed in some detail by Eelsalu et al. (2025), we present here only a compendium of the overall wave climate and local marine weather at the site. Waves created in the Baltic proper may affect only the northern sector of the Gulf of Riga. Therefore, most of this gulf, including the vicinity of the experiment site, has its own wave regime – mostly locally generated waves – that is detached from wave properties in the Baltic proper. As a consequence, the wave climate in the Gulf of Riga (Eelsalu et al., 2014; Najafzadeh et al., 2024) is clearly milder than in the Baltic proper (Björkqvist et al., 2018). As waves are mostly locally generated, the well-known predomination of western winds leads to a somewhat milder wave climate in the west and more intense waves in the eastern part of the gulf. Owing to the relatively small size of the gulf, waves are typically not only lower but also shorter than in the Baltic proper, and saturated wave fields often occur. The long-term average significant wave height is below 0.8 m and wave periods are usually 2–5 s. Still, very severe wave conditions may occur in this gulf that has a strongly intermittent wave climate similar to the rest of the Baltic Sea. For example, it is likely that the significant wave height exceeded 4 m in the eastern part of the gulf in the January 2005 storm and even 6 m in 1967 (Björkqvist et al., 2018; Najafzadeh et al., 2024).

The properties of marine weather near the experiment site were tracked using both measured and modelled data sets. Properties of waves and currents were recorded hourly by a SmartBuoy device operated by the Latvian Institute of Aquatic Ecology (LHEI) near the experiment site at 57°19.199′N, 24°21.813′E over the entire experiment. The buoy was deployed in 15 m deep water about 1.5 km from the experiment site (Figure 1). In this analysis we only use wave data estimated by a Wave and Tide Sensor 5218 (Aanderaa, Norway, one of the instruments on the SmartBuoy), based on pressure time series measured over 120 s. As this time interval is by an order of magnitude shorter than intervals that are commonly used to evaluate wave properties (15–30 min.), the time series of wave properties may have relatively large scatter.

To provide an improved description of the marine weather during the experiment, we also employed modelled time series of wave properties. These were generated using a nested SWAN model (Booij et al., 1999) forced by

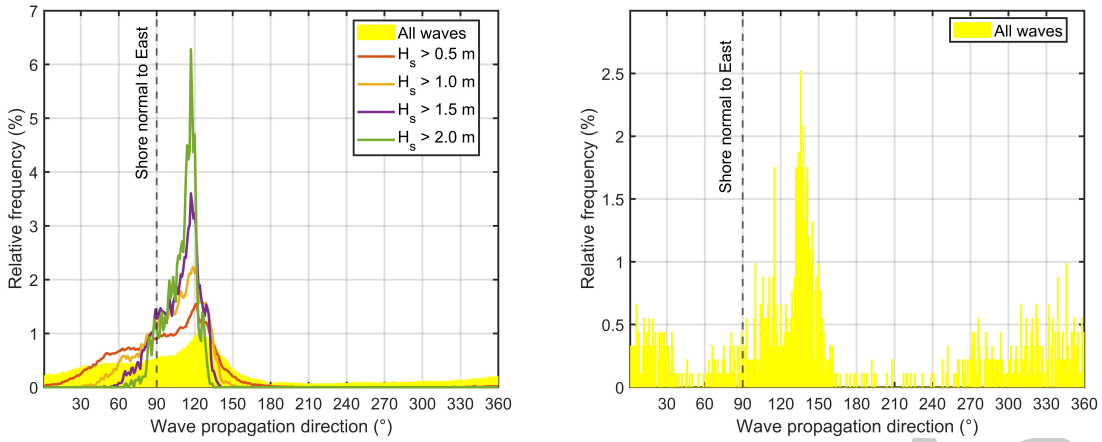


Figure 4. Empirical probability density distribution (relative frequency) of propagation directions (to where waves are propagating, clockwise from the North) of modelled waves in the grid cell closest to the experiment site (Figure 1) 1990–2022 (left panel) and during the experiment (right panel). Direction 90° thus means that waves propagate to the shore exactly along the shore normal and direction 120° corresponds to the approach angle of 30°.

ERA5 winds (Hersbach et al., 2020). This model was applied for the entire Baltic Sea with a spatial resolution of about 3 nautical miles and then for the Gulf of Riga with a spatial resolution of 1 nautical mile (Giudici et al., 2023; Najafzadeh et al., 2024). The model was carefully tuned for Baltic Sea conditions and validated against recorded wave data from the Baltic proper and Gulf of Finland by Giudici et al. (2023) and for the Gulf of Riga by Najafzadeh et al. (2024). Wave parameters for this study were retrieved for a grid cell located in 8.6 m deep water about 600 m from the measurement location at 24°22′48″E, 57°19′30″N (Figure 1).

The long-term average modelled significant wave height H_S at this location is 0.5 m. The hourly modelled H_S fluctuated around this value in July (Eelsalu et al., 2025), was mostly 0.2–0.3 m on the first days of August, increased up to 0.8 m on 7 August (Figure 3) and decreased to 0.1–0.3 m in the rest of August, but was up to 0.4 m for a short time on 25 August. The end of August (27–31 August) and beginning of September (02 September) had H_S between 0.5 and 1 m. After this, H_S was around 0.3–0.4 m on 1–6 September but again reached 1 m at the very end of the experiment on 7 September. The course of estimates of H_S by the SmartBuoy qualitatively followed the modelled H_S (Figure 3). Frequent deviations of the H_S values by the SmartBuoy from the modelled ones most likely stem from the short time interval used by the SmartBuoy to evaluate the wave height. Both modelled and recorded (by the SmartBuoy) peak wave periods were mostly 2–4 s. They generally followed the course of wave heights and reached 6 s at the end of August. Such long wave periods are relatively uncommon in the Gulf of Riga (Najafzadeh et al., 2024) and were created by moderate to strong NW winds that have the longest fetch for the study area.

The SmartBuoy did not record wave directions. The modelled waves predominantly arrived at the measurement location from the west and west-north-west (WNW), with a few short events with waves from the North (Figure 3). Recorded wind data from the meteorological station at Skulte (57.300644°N, 24.412278°E) located next to the Port of Skulte and operated by the Latvian Environment, Geology and Meteorology Centre (LEGCM) indicate that south-eastern (SE) winds predominated during the very calm time from 7 August until almost the end of the month, on some occasions probably under rapidly rotating wind directions between the south and east. Waves excited by these winds were propagating in the offshore direction. During stronger wave events at the end of August and in September, waves arrived either from the west, WNW or north-west (NW) (that is, from the direction of the longest fetch for the experiment site). Waves from these directions propagated to directions from 90° to 120° in the above-described framework (counted clockwise from the North). It is likely that these waves have already experienced significant refraction-driven rotation that seems to be common for coastal areas of the Gulf of Finland (Männikus et al., 2022, 2024).

The directional distribution of modelled waves (1990–2022) extracted from the simulations of Giudici et al. (2023) and Najafzadeh et al. (2024) shows a strong dependence on the wave heights (Figure 4, left). As the location of the relevant wave model grid cell is only about 1 km from the shore, it is natural that the proportion of waves propagating to all western directions is very small and these waves are also small. The directional distribution of all waves that propagate towards the shore has a clear peak for WNW waves (propagation direction about 120°) and a wide plateau for waves from SSW to NW. Waves from

In Press

the North are less frequent. This distribution changes considerably if only higher waves are considered. It becomes narrower for higher waves. The proportion of waves from SW rapidly decreases if the modelled $H_s > 1$ m and becomes negligible for modelled $H_s > 2$ m. Almost all such waves arrive from the northern direction. Interestingly, the most frequent propagation direction of waves for all wave heights varies in a narrow range from 117° to 120°. This distribution for the experiment period has the same general appearance but the most frequent waves propagate to the direction of 135° (and arrive from NW) and waves also frequently propagate to the NW, north or even ENE. These wave systems, however, have very small heights (Figure 3). Therefore, the most frequent waves among higher modelled waves arrive from the direction of about 300° and thus reach the experiment site at an angle of about 30° with respect to the shore normal.

3. Results

3.1 Wave directions from ADV recordings

The directional distribution of all motions recorded by the ADV (Figure 5) is almost isotropic and contains three flat peaks for water flow to the following directions: (i) 100° to 170° (to the SE and adjacent directions), (ii) 280° to 310° (to the WNW and adjacent directions), and (iii) from 340° to 10° (almost to the North). The maximum frequency of occurrence is 0.0042 at the peak at WNW and the minimum 0.0015 at about −210° (WSW) while the average is 1/360 = 0.00278.

Even though the peaks have very moderate heights, this structure matches the well-known bi-directional structure of moderate and strong winds in the area (Soomere and Keevallik, 2001; Soomere, 2003). As the study site is located near the eastern shore of the Gulf of Riga, consequential waves may arrive at this location only from the western directions. The peaks at SE and around the North therefore reflect forward water velocities under the crests of arriving waves and the peak at the WNW represents reverse velocities under wave troughs (Figure 6).

The directional distribution of even very moderate speeds, starting from values as low as 0.03 m/s, is much more anisotropic. The smaller peaks at about 150° (SSE) and 350° (N-NNE) become slightly more pronounced for speeds above 0.03 m/s and 0.05 m/s but become much lower for speeds above 0.1 m/s and disappear for speeds >0.15 m/s. Therefore, only very low waves in which the near-bottom flow speed does not exceed about 0.03 m/s have arrived from the south-south-west (SSW) and adjacent directions during the study period.

The directional distribution of higher speeds (>0.1 m/s) is strongly anisotropic. Waves that have excited such speeds have arrived only from a narrow range of directions from 270° to 320° (from the West to NW) and propagated to the directions from 90° to 140°. This observation is consistent with the conjecture of Eelsalu et al. (2024) that waves from a narrow range of ±15° from one or two predominant directions create up to 90% of the alongshore sediment transport. The share of such waves is fairly small: only 8.22% of all recordings exceeded 0.15 m/s, 2.09% were ≥0.3 m/s and 0.36% were ≥0.5 m/s (Eelsalu et al., 2025). This pattern also matches the wave data recorded near Skulte by the SmartBuoy and the modelled data: wave directions during relatively high waves were predominantly from the west to WNW (Figure 3),

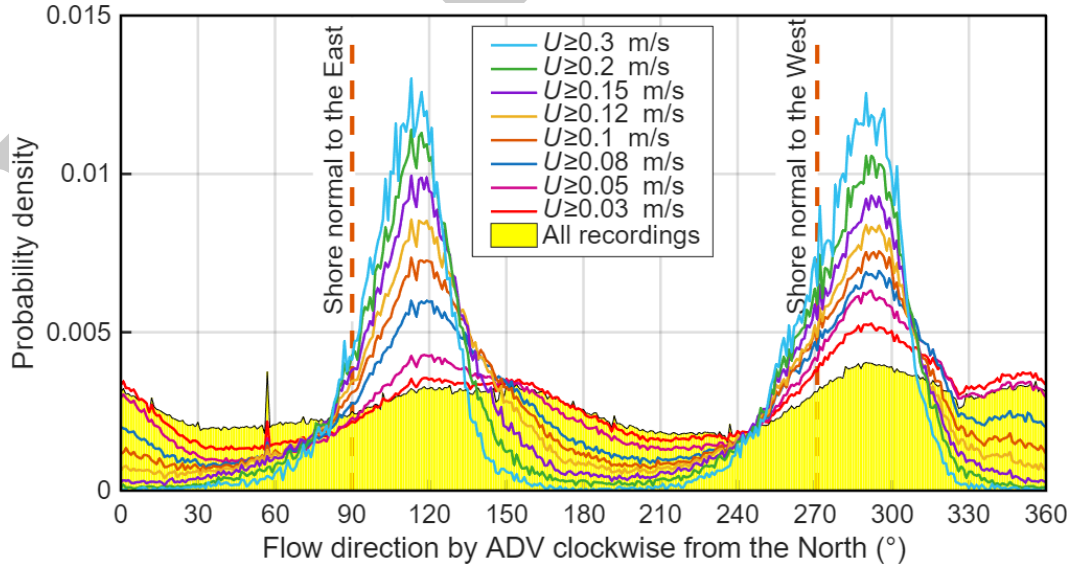


Figure 5. Empirical probability density distributions (relative frequency of occurrence) of directions of water velocity (= to where water is moving) recorded by the ADV with a directional resolution of 1° (360 bins). The directions are counted clockwise from the North so that East = 90°, South = 180°, West = 270°, and North = 0°/360°.

Preprint

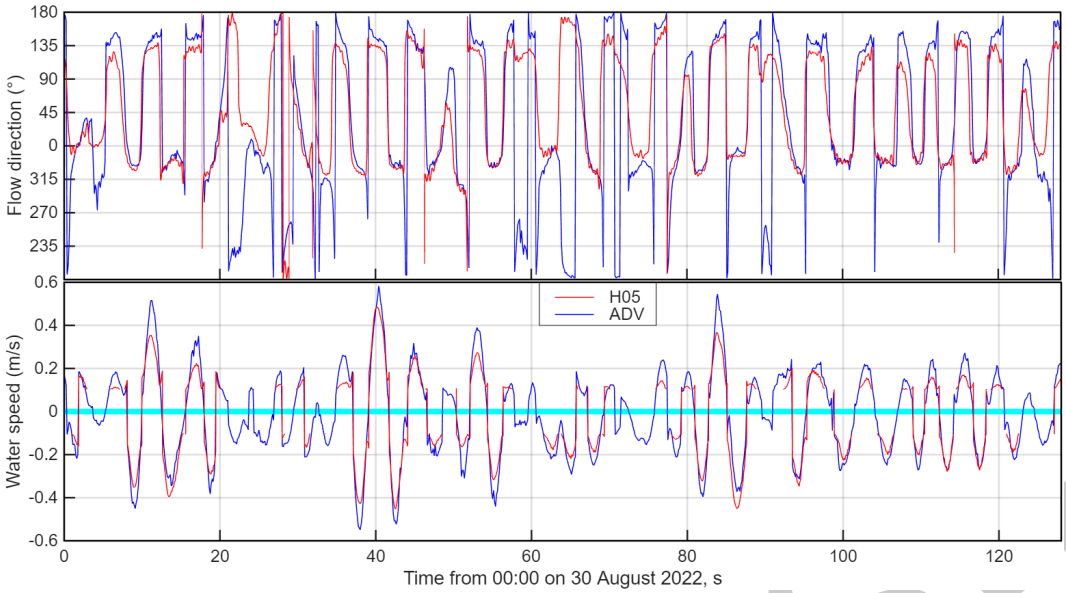


Figure 6. Time series of flow direction (upper panel) and speed (lower panel) measured using the ADV (blue) and the neighbouring hydromast H05 from 00:00 to 00:02 (128 s, ADV burst 1367) on 30 August. Speed recordings by hydromasts are smoothed over 8 subsequent values. The values of water speed <0.1025 m/s from this hydromast are not reliable (Eelsalu et al., 2025) and not displayed. Onshore-directed water speed under wave crests is displayed as positive and water speed under troughs as negative.

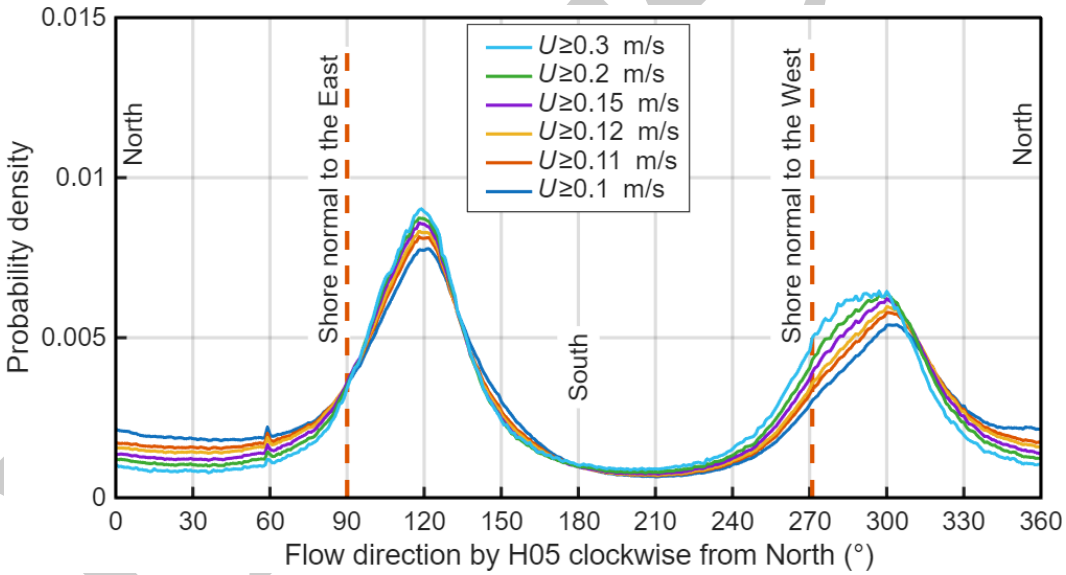


Figure 7. Empirical probability density distributions (relative frequency of occurrence) of water flow directions recorded by hydromast H05 for water speeds exceeding a set of thresholds (see the legend), counted in degrees clockwise from the North = 0°/360° and presented with a resolution of 1°. The slopes of curves for different speed thresholds in the range of probabilities from 1/360 (the average level) to 3/360 (near the peak) were in the range from 0.00015 to 0.00022 for the left-hand slope of the peak and from −0.00017 to −0.0025 for the right-hand slope. The right-hand slopes for each threshold exceed the left-hand slopes by at least 10%.

whereas a relatively large number of low waves propagated to the NNW and adjacent directions (Figure 4).

It is natural to associate the direction of water speed with the direction where the relevant wave is propagating. In this context, the described distributions match the similar distributions for modelled wave directions. The main difference compared to the directional distribution of recorded waves is the presence of flow directions under wave troughs opposite to the wave propagation direction, which leads to an almost symmetric two-peak directional

distribution of all ADV-measured velocities. The distributions for larger flow speeds become gradually more similar to the distributions of modelled wave directions for H_s larger than about 1 m. Thus, waves that create larger flow speed also most frequently arrive from the direction of about 300° and thus reach the experiment site at an angle of about 30° with respect to the shore normal. While it is often assumed that higher waves produce larger near-bottom water speed, this assumption is not true in many coastal segments, including the measurement site. The reason is the strongly nonlinear dependence of wave-driven motions on wave periods for some water depths. For example, the maximum near-bottom speed created at a depth of 4 m by a linear wave with a height of 0.5 m substantially depends on the wave period. This maximum speed is only 0.019 m/s for a wave with a period of 2 s but 0.151 m/s for a wave with a period of 4 s and 0.302 m/s for a wave with a period of 6 s. The larger the threshold, the narrower the peaks are, signalling that such waves tend to arrive from a narrow range of directions. All these distributions have a steep slope for directions more to the North from NNW and a gentler slope for directions from the NW to further south.

It is likely that a blip at 57° reflects ship wakes generated in the entrance channel to the Port of Skulte and propagating to the ENE (Eelsalu et al., 2025). It is clearly present also in similar distributions retrieved from hydromast recordings. Notably, this blip is much lower in the distribution of backward flow distributions. This feature may represent the asymmetric nature of ship wakes that often have a steeper front side.

3.2 Flow directions from the hydromast adjacent to the ADV

Hydromast H05 was mounted immediately adjacent to the ADV (Figure 2). The recordings of flow speed and direction contain 155,539,653 entries, sampled at 50 Hz over 36 days from 00:00 on 02 August until 24:00 on 07 September. Flow directions retrieved from the ADV and from its closest hydromast show very good match (Figure 6). The recorded directions almost coincide in both the incoming and outgoing phase of each single wave crest. The mismatch in these directions is usually only a few degrees. A larger mismatch occurs during the short instants when the flow induced under wave crests stops and starts to reverse. These instants are represented as zero-crossings of flow speed in Figure 6. This mismatch is natural because water speed is very small and the direction of the flow is poorly defined during this phase of the waves. Notably, water flow directions from the two devices also show a very good match in situations beyond the validated range of hydromasts 0.15–1.0 m/s (Egerer et al., 2024), down to flow speeds 0.1–0.11 m/s. This feature indicates that the range of validity of flow direction recordings by hydromasts is wider than for water speed recordings.

The probability density distributions for directions of these flow speeds that are reliably recorded by hydromast H05 from 03 August to 07 September (Figure 7) match all core features of these distributions of ADV-recorded data (Figure 5). A characteristic high and narrow peak is present in all relative probability density distributions of water speeds of ≥0.1 m/s at a direction of 120°. This peak evidently reflects forward motions under crests of incoming waves approaching from the WNW (and propagating to the ESE). A wider peak at directions 270°–300° reflects reverse (backward) water motions under wave troughs from the ESE to the NNW. The peaks become gradually narrower when only larger water speeds (higher or longer waves) are considered. The maxima of both peaks are located exactly at the same direction (forward motions at 120°, reverse flow at 300°). All peaks are slightly asymmetric: the slope is steeper for forward motions with a direction >120° and reverse motions with a direction >300°, and gentler for forward motions with a direction <120° and reverse motions with a direction <300°. Most importantly, both recordings demonstrate that most of the waves of appreciable height (generating near-bottom velocities ≥0.1 m/s) approach at an angle of about 30° with respect to the shore normal.

Interestingly, even the small blip at 59° that may reflect ship wakes generated by vessels calling at the Port of Skulte is reflected in the directional distributions of hydromast data. It is likely that the slightly different locations of these blips between the hydromast and the ADV (57°) reflect the uncertainty in specification of directions of the devices. This blip is missing in hydromast-recorded reverse flow data apparently because of the asymmetric shape of ship-induced waves that often have a relatively steep front. It may thus occur that only forward motion in these waves is reliably recorded by the hydromasts.

3.3 Flow directions from the set of hydromasts

The orientation of wave crests and thus the wave-generated flow direction in short-crested wave systems may considerably vary over even small distances. While horseshoe-like patterns sporadically appear in deep water (Annenkov and Shrira, 1999), crescent wave patterns are common at smaller depths (Su and Green, 1984; Kristiansen et al., 2005). The wave climate of the Baltic Sea and the Gulf of Riga is dominated by locally generated wind-seas (Najafzadeh et al., 2024) that often have short-crested appearance, and the experiment site is located in relatively shallow water. To try to quantify spatial variations in the directional structure of wave-driven near-bottom velocities, we compare empirical probability density distributions of flow directions for four devices at the outer corners of the frame. These devices are located 20 m from each other and 14 m from hydromast H05 and the ADV. For this comparison, we only employed recordings in which the flow speed exceeded the reliability threshold evaluated by Eelsalu et al. (2025).

In Press

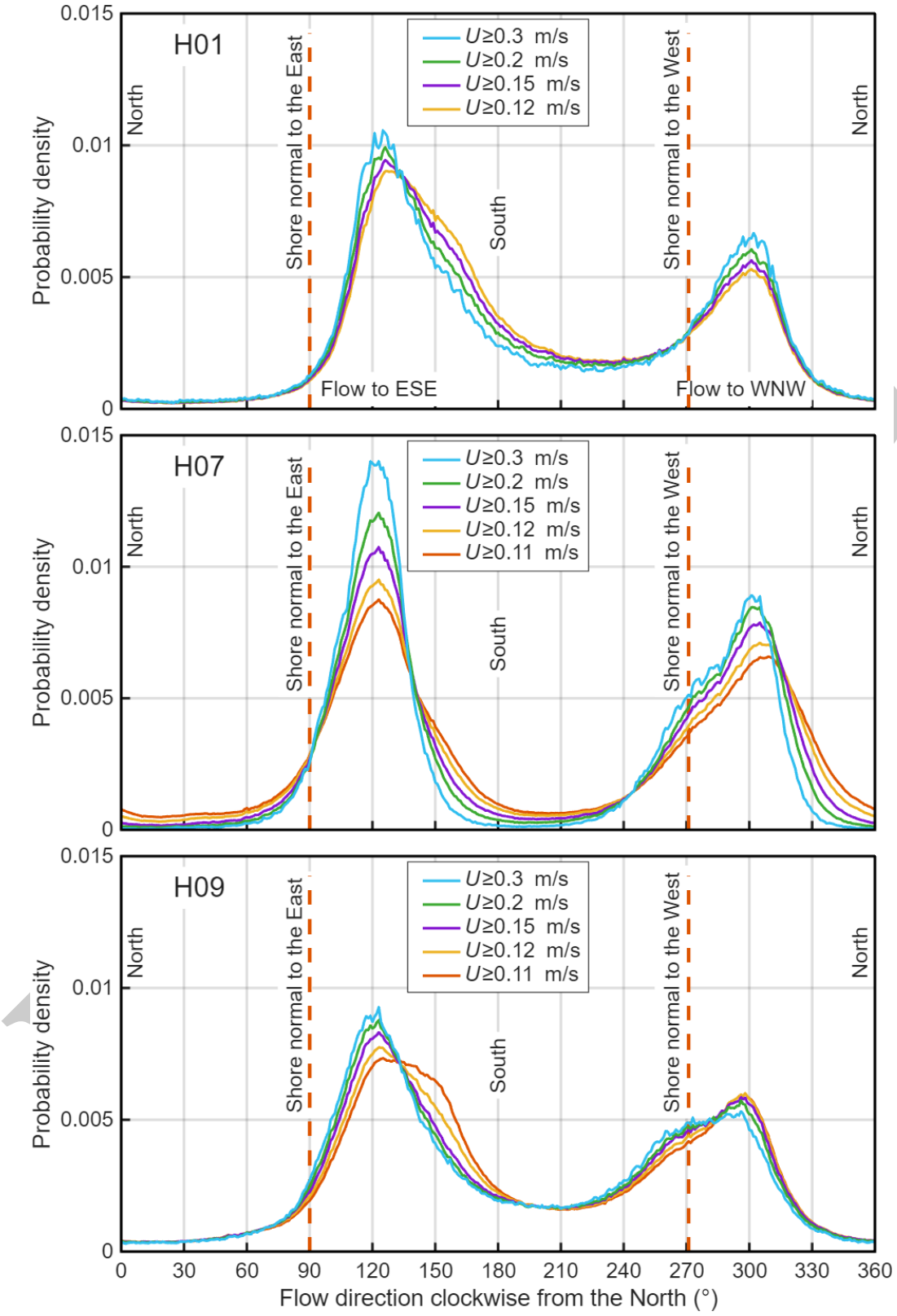


Figure 8. Empirical probability density distributions (relative frequency of occurrence) of water flow directions recorded by hydromast H01 at the northernmost corner of the frame, H07 in the westernmost corner, and H09 in the southernmost corner of the frame (Figure 1). Recordings of water speed are reliable from 0.1075 m/s for H07 and H09, and from 0.1175 m/s for H01 (Eelsalu et al., 2025).

As expected, the overall structure of all directional distributions is the same as for the ADV and hydromast H05. This feature is true for flow speeds exceeding different thresholds from 0.11 m/s (0.12 m/s for H01) to 0.3 m/s (Figure 8).

Recordings from all devices confirm that higher waves most frequently arrive from the direction of 300° (close to WNW) and propagate in the direction of about 120° (to the ESE), while the backward flow goes most frequently in the WNW direction. A large portion of such motions arrive from a relatively narrow directional range of ±15–20° from this most frequent direction.

The probability density distributions of water velocity directions have also certain specific features for some hydromasts (Figure 8). Unlike similar distributions in Figures 5 and 7, the peaks at 120° have a steeper slope at directions <120° and a less steep slope at directions >120° in distributions constructed from the recordings of hydromasts H01 and H09. This feature is even more pronounced for the peak representing the backflow at 300°. Moreover, lower flow speeds tend to be more frequently directed to 150°–180°, that is, to the ESE and almost to the South in recordings of H09. The peak for backward flow from recordings of H09 is lower than based on the data from other devices.

On the contrary, the peak at 120° has a shape similar to the one based on the ADV and hydromast H05. The heights of both peaks for this device are close to those derived from the ADV measurements. They are clearly higher than those based on recordings of other devices. As a minor feature, the blip that apparently reflects ship-generated waves is missing in all recordings represented in Figure 8. This blip is visible in recordings of some other hydromasts, such as H02 and H06 (not shown).

4. Discussion and conclusions

A dedicated experiment near the eastern shore of the Gulf of Riga, the third largest subbasin of the Baltic Sea, was performed to evaluate the typical approach direction of waves of appreciable height. The modelled data for 1990–2022 suggest that such waves most frequently arrive from the west-north-west (direction 300° clockwise from the North) and very infrequently from other directions. Such waves typically approach the shore at an angle of about 30° with respect to the shore normal.

The experiment reveals that most waves of appreciable height (more specifically, waves that excited appreciable near-bottom speed) approached the shore at an angle of $30 \pm 15°$ with respect to the shore normal during the measurements. This property becomes evident in recordings of all used devices (ADV and hydromasts) starting from flow speeds about 0.1 m/s. The exact proportion of such waves and the probability density of occurrence of such waves from different directions varies to some extent at locations separated by 10–30 m from each other.

The relatively short measurement period – five weeks in August–September 2022 – does not contain any strong storms and is characterised by somewhat lower than long-term average significant wave height and slightly atypical directional structure of wave fields in the study site. The presented results still suggest that higher or longer than average wave fields tend to approach from a narrow range of directions. The larger the wave-driven water speeds are, the narrower is this range. Even though the measurements only covered five weeks, the empirical probability density distribution of the occurrence of waves from different directions during the experiment matches well the similar distribution for modelled waves over >30 years 1990–2022. It is thus likely that the wave regime during the experiment represents well the long-term wave climate in the area.

This conjecture reinforces the core result of this study: there is a clear predominant wave approach direction in the study area such that higher waves approach the shore at an angle of 30° with respect to the shore normal. Waves that approach the shore at a large angle (but below about 45°, Ashton and Murray, 2006) with respect to the shore normal at the breaker line generate alongshore sediment transport that can be several times as intense as similar transport created by waves that approach the shore at a smaller angle. As the water depth in our experiment site is such that the highest recorded waves are close to breaking, the observed approach angle will not change much when storm waves propagate from this site to the breaker line. Even though refraction continues in the breaker zone, wave properties at the breaker line are often used to evaluate the properties of wave-driven transport (e.g., USACE, 2002).

This predominance of large wave approach angles, albeit established for a single location, seems to be characteristic for many coastal segments of the eastern and south-eastern Baltic Sea (Eelsalu et al., 2024; Soomere et al., 2024) where the orientation of the coast with respect to the predominant wind and wave directions resembles the orientation at our measurement site. It explains why sediment transport along several segments of the eastern Baltic Sea is unusually intense (Knaps, 1966; Ulsts, 1998; Soomere and Viška, 2014; Jankowski et al., 2024; Soomere et al., 2025) even though the Baltic Sea wave climate is mild (Björkqvist et al., 2018) and the wave climate of its subbasins is even milder. It also carries a strong message to the nearshore communities and coastal managers who should expect unusually strong wave-driven sediment transport in this and similar coastal areas, including in coastal segments that may experience large approach angles during periods of strong waves owing to climate change as described in the Introduction, with direct consequences in terms of coastal exposedness and vulnerability.

The match of predominant wave directions near the study site and directions of wave-driven water velocities retrieved from the measurements can be first interpreted

In Press

as an argument for the validity of the experiments. However, this match also signals that widely used wave models (SWAN in our study) with a moderate spatial resolution of about 1 nautical mile and forced by commonly available reanalysis wind products (ERA5 in our study) adequately replicate wave directions (and apparently other wave properties) almost until the breaker line. This conjecture to some extent questions efforts towards even better resolution wave simulations in coastal areas with relatively simple geometry and bathymetry.

We also stress that wave heights, periods or large wave-driven water speeds alone are usually not the main driver of sediment transport or coastal evolution. More likely it is an important constituent of changes to the coast that depend on a variety of other factors and drivers, from the actual pattern of a storm and the presence of elevated water level (that are often supported by set-up of waves that arrive at the shore at a small angle) to the sediment composition and sand capacity near the waterline and in the foredunes.

A question that remains open is what causes differences in the empirical probability distributions of flow directions at different locations. On the one hand, it is most likely that part of it reflects natural variability of the near-bottom velocity field under short-crested wave conditions and actual somewhat irregular seabed. Even though the seabed was generally flat, it contained several features with a height of 10–20 cm and several stones of the same size. Such features may easily give rise to systematic local variations in the velocity fields, including changes to the directional structure of near-bottom motions. On the other hand, we observed significant variations in the heights of the peaks of the empirical probability density distributions of directions of incoming waves and reverse flow for water speed over certain thresholds. The varying rate of this difference for different hydromasts may stem from intrinsic features of devices of this kind that do not become evident in direct comparisons of single data points but may cumulate in terms of statistical distributions. For example, different level of skewness of the main peak of the probability density distributions for some hydromasts may reflect the tendency of the devices to slightly "prefer" some directions. However, it is safe to say, based on the performed analysis, that hydromast devices can be successfully employed to record the main properties of oscillatory flows. Even though their internal features may add small bias to the probability distribution of flow properties, the overall flow structure in terms of its speed and direction, and its main statistical features are captured reliably.

The core value of hydromasts is that they are inexpensive relative to instruments like the ADV, easy to handle, synchronise and mount, and able to provide properties of the water flow at high temporal and spatial resolution. For this reason, they were preferable for the analysis of spatial variations in flow speeds (Eelsalu et al., 2025) and for detection of the course and orientation of ship wakes in shallow water (Rätsep et al., 2021). The presented results demonstrate that the hydromasts can be reliably used to study wave directions in such demanding conditions of almost breaking waves even though there may be certain quantitative differences between them in terms of probability distributions of recorded directions. Their use can meet one of the biggest criticisms of using cheap pressure sensors to measure wave properties (as many people do) that there is no information about wave direction, and we know that is particularly important in fetch limited environments and in the nearshore zone. They can thus provide inexpensive and largely reliable information about wave directions in shallow water where other measurement methods are either inappropriate or require at least three synchronised pressure sensors (Howell, 1998; Fernandes et al., 2000). Because they are cheap, wide spatial coverage using many single-direction measuring devices could be achieved for basically the same cost as a single ADV.

Acknowledgements

The research was co-supported by the Estonian Research Council (grants PRG1129, PRG3038, and PSG940), the European Economic Area (EEA) Financial Mechanism 2014–2021 Baltic Research Programme (project SolidShore, grant EMP480), CETPartnership project FROST via Estonian Research Council subgrant MOB3PRT25, Tallinn University of Technology bridging grants GFLTME24 and GFLTME25, and the European Union through H2020 project ILIAD (grant agreement No. 101037643).

We are deeply grateful to the Latvian Institute of Aquatic Ecology (LHEI) for providing the SmartBuoy data during the experiment period and to Latvian Environment, Geology and Meteorology Centre (LEGCM) for providing access to meteorological data recorded at Skulte.

Declaration of generative AI use

The authors did not use any AI models during preparation of the manuscript.

Authors' contribution

Tarmo Soomere: Conceptualisation, Methodology, Validation, Formal analysis, Investigation, Resources, Visualisation, Writing – original draft and final manuscript, Supervision, and Project Administration. Maris Eelsalu: Validation, Formal analysis, Visualisation, and Writing – original draft. Kevin Parnell: Conceptualisation, Investigation, Data curation, Writing – final manuscript. Laura Piho: Formal analysis, Investigation, Field work, Data curation. All authors have read and agreed to the published version of the manuscript.

Under review

Data availability

The recorded hydromast data are available on request from Laura Piho. The ADV data are available on request from Kevin Parnell.

Conflict of interest

None declared.

References

Annenkov, S.Y., Shrira, V.I., 1999. *Sporadic wind wave horseshoe patterns*. Nonlinear Proc. Geoph. 6 (1), 27–50. https://doi.org/10.5194/npg-6-27-1999

Ashton, A.D., Murray, A.B., 2006. *High-angle-wave instability and emergent shoreline shapes: 1. Modeling of sandwaves, flying spits, and capes*. J. Geophys. Res.-Earth. 111 (F4), F04011. https://doi.org/10.1029/2005JF000422

Bierstedt, S.E., Hünicke, B., Zorita, E., 2015. *Variability of wind direction statistics of mean and extreme wind events over the Baltic Sea region*. Tellus A 67, 29073. https://doi.org/10.3402/tellusa.v67.29073

Booij, N., Ris, R., Holthuijsen, L., 1999. *A third generation wave model for coastal regions, 1: model description and validation*. J. Geophys. Res.-Oceans 104 (C4), 7649–7666. https://doi.org/10.1029/98JC02622

Björkqvist, J.-V., Lukas, I., Alari, V., van Vledder, P.G., Hulst, S., Pettersson, H., Behrens, A., Männik, A., 2018. *Comparing a 41-year model hindcast with decades of wave measurements from the Baltic Sea*. Ocean Eng. 152, 57–71. https://doi.org/10.1016/j.oceaneng.2018.01.048

Carter, R.W.G., 2002. *Coastal environments*. 8th edn., Acad. Press, Amsterdam, 617 pp.

Casas-Prat, M., Sierra, J.P., 2010. *Trend analysis of wave storminess: wave direction and its impact on harbour agitation*. Nat. Hazard. Earth Sys. 10 (11), 2327–2340. https://doi.org/10.5194/nhess-10-2327-2010

Casas-Prat, M., Wang, X.L.L., 2020. *Projections of extreme ocean waves in the Arctic and potential implications for coastal inundation and erosion*. J. Geophys. Res.-Oceans 125 (8), e2019JC015745. https://doi.org/10.1029/2019JC015745

Charles, E., Idier, D., Delecluse, P., Déqué, M., Le Cozannet, G., 2012a. *Climate change impact on waves in the Bay of Biscay, France*. Ocean Dynam. 62 (6), 831–848. https://doi.org/10.1007/s10236-012-0534-8

Charles, E., Idier, D., Thiébot, J., Le Cozannet, G., Pedreros, R., Ardhuin, F., Planton, S., 2012b. *Present wave climate in the Bay of Biscay: Spatiotemporal variability and trends from 1958 to 2001*. J. Climate 25 (6), 2020–2039. https://doi.org/10.1175/JCLI-D-11-00086.1

Dolphin, T.J., Vincent, C.E., Wihsgott, J., Belhache, M., Bryan, K.R., 2011. *Seasonal rotation of a mixed sand-gravel beach*. J. Coastal Res. Special Issue 64, 65–69.

Echevarria, E.R., Hemer, M.A., Holbrook, N.J., Marshall, A.G., 2020. *Influence of the Pacific-South American modes on the global spectral wind-wave climate*. J. Geophys. Res.-Oceans 125 (8), e2020JC016354. https://doi.org/10.1029/2020JC016354

Eelsalu, M., Org, M., Soomere, T., 2014. *Visually observed wave climate in the Gulf of Riga*. [In:] *The 6th IEEE/OES Baltic Symposium Measuring and Modeling of Multi-Scale Interactions in the Marine Environment, May 26–29, 2014, Tallinn Estonia*, IEEE Conference Publications. https://doi.org/10.1109/BALTIC.2014.6887829

Eelsalu, M., Piho, L., Aigars, J., Kelpšaitė-Rimkienė, L., Kondrat, V., Kruusmaa, M., Parnell, K.E., Ristolainen, A., Šakurova, I., Skudra, M., Viška, M., Soomere, T., 2025. *Exponential distribution of wave-driven near-bed water speeds under short-crested waves: a case study in the eastern Gulf of Riga, the Baltic Sea*. Proc. Est. Acad. Sci. 74 (1), 23–42. https://doi.org/10.3176/proc.2025.1.03

Eelsalu, M., Soomere, T., 2026. *Disruptions in alongshore sediment transport on sedimentary shores of the Baltic Sea driven by changes in prevailing wave fields*. Ocean Eng. 356 (1), 124952. https://doi.org/10.1016/j.oceaneng.2026.124952

Eelsalu, M., Soomere, T., Jankowski, M.Z., 2024. *Climate change driven alongshore variations of directional forcing of sediment transport on the eastern Baltic Sea coast*. J. Coastal Res. 113 (Sp. Iss.), 256–260. https://doi.org/10.2112/JCR-SI113-051.1

Egerer, M., Ristolainen, A., Piho, L., Vihman, L., Kruusmaa, M., 2024. *Hall effect sensor based low cost flow monitoring device: design and validation*. IEEE Sens. J. 24 (5), 5986–5997. https://doi.org/10.1109/JSEN.2024.3354194

Elshinnawy, A.I., Antolínez, J.A.A., 2023. *A changing wave climate in the Mediterranean Sea during 58-years using UERRA-MESCAN-SURFEX high-resolution wind fields*. Ocean Eng. 271, 113689. https://doi.org/10.1016/j.oceaneng.2023.113689

Fernandes, A.A., Sarma, Y.V.B., Menon, H.B, 2000. *Directional spectrum of ocean waves from array measurements using phase/time/path difference methods*. Ocean Eng. 27 (4), 345–363. https://doi.org/10.1016/S0029-8018(99)00024-4

Flor-Blanco, G., Alcántara-Carrió, J., Jackson, D.W.T., Flor, G., Flores-Soriano, C., 2021. *Coastal erosion in NW Spain: Recent patterns under extreme storm wave events*. Geomorphology 387, 107767. https://doi.org/10.1016/j.geomorph.2021.107767

Ghanavati, M., Young, I.R., Kirezci, E., Liu, J., 2024. *The impact of long-term changes in ocean waves and storm*

In Press

surge on coastal shoreline change: a case study of Bass Strait and south-east Australia. Nat. Hazard. Earth Sys. 24 (6), 2175–2190. https://doi.org/10.5194/nhess-24-2175-2024

Giudici, A., Jankowski, M.Z., Männikus, R., Najafzadeh, F., Suursaar, Ü., Soomere, T., 2023. *A comparison of Baltic Sea wave properties simulated using two modelled wind data sets*. Estuar. Coast. Shelf S. 290, 108401. https://doi.org/10.1016/j.ecss.2023.108401

Gómez, M., Aránguiz, R., Mäll, M., 2024. *Analysis of climate change and climate variability impacts on coastal storms induced by extratropical cyclones: a case study of the August 2015 storm in central Chile*. Coast. Eng. J. 66 (4), 617–636. https://doi.org/10.1080/21664250.2024.2392355

Harley, M.D., Turner, I.L., Kinsela, M.A., Middleton, J.H., Mumford, P.J., Splinter, K.D., Phillips, M.S., Simmons, J.A., Hanslow, D.J., Short, A.D., 2017. *Extreme coastal erosion enhanced by anomalous extratropical storm wave direction*. Sci. Rep.-UK 7, 6033. https://doi.org/10.1038/s41598-017-05792-1

Hemer, M.A., Church, J.A., Hunter, J.R., 2010. *Variability and trends in the directional wave climate of the Southern Hemisphere*. Int. J. Climatol. 30 (4), 475–491. https://doi.org/10.1002/joc.1900

Hersbach, H., Bell, B., Berrisford, P., Hirahara, S., Horanyi, A., Munoz-Sabater, J., Nicolas, J., Peubey, C., Radu, R., Schepers, D., Simmons, A., Soci, C., Abdalla, S., Abellan, X., Balsamo, G., Bechtold, P., Biavati, G., Bidlot, J., Bonavita, M., De Chiara, G., Dahlgren, P., Dee, D., Diamantakis, M., Dragani, R., Flemming, J., Forbes, R., Fuentes, M., Geer, A., Haimberger, L., Healy, S., Hogan, R.J., Holm, E., Janiskova, M., Keeley, S., Laloyaux, P., Lopez, P., Lupu, C., Radnoti, G., de Rosnay, P., Rozum, I., Vamborg, F., Villaume, S., Thepaut, J.N., 2020. *The ERA5 global reanalysis*. Q. J. Roy. Meteor. Soc. 146 (730), 730, 1999–2049. https://doi.org/10.1002/qj.3803

Howell, G.L., 1998. *Shallow water directional wave gages using short baseline pressure arrays*. Coast. Eng. 35 (1–2), 85–102. https://doi.org/10.1016/S0378-3839(98)00031-3

Jankowski, M.Z., Soomere, T., Parnell, K.E., Eelsalu, M., 2024. *Alongshore sediment transport in the eastern Baltic Sea*. J. Coast. Res. 113 (Sp. Iss.), 261–265. https://doi.org/10.2112/JCR-SI113-052.1

Kamphuis, J.W., 1991. *Alongshore sediment transport rate*. J. Waterw. Port C.-ASCE 117, 624–640. https://doi.org/10.1061/(ASCE)0733-950X(1991)117:6(624)

Kilar, H., Amarouche, K., Akpinar, A., 2025. *Wave storm impacts on shoreline evolution: A case study of Iztuzu beach*. Ocean Coast. Manage. 267, 107748. https://doi.org/10.1016/j.ocecoaman.2025.107748

Knaps, R.J., 1966. *Sediment transport near the coasts of the Eastern Baltic*. [In:] *Development of sea shores under the conditions of oscillations of the Earth's crust*, Valgus, Tallinn, 21–29 (in Russian).

Kristiansen, O., Fructus, D., Clamond, D., Grue, J., 2005. *Simulations of crescent water wave patterns on finite depth*. Phys. Fluids 17 (6), 064101. https://doi.org/10.1063/1.1920351

Larson, M., Hoan, L.X., Hanson, H., 2010. *Direct formula to compute wave height and angle at incipient breaking*. J. Waterw. Port C.-ASCE 136 (2), 119–122. https://doi.org/10.1061/(ASCE)WW.1943-5460.0000030

Männikus, R., Soomere, T., Najafzadeh, F., 2022. *Refraction may redirect waves from multiple directions into a harbour: a case study in the Gulf of Riga, eastern Baltic Sea*. Est. J. Earth Sci. 71 (2), 80–88. https://doi.org/10.3176/earth.2022.06

Männikus, R., Wang, W.W., Eelsalu, M., Najafzadeh, F., Bihs, H., Soomere, T., 2024. *Modelling suitable layout for a small island harbour: a case study of Ruhnu in the Gulf of Riga, eastern Baltic Sea*. Latv. J. Phys. Tech. Sci. 61 (6), 3–24. https://doi.org/10.2478/lpts-2024-0040

McSweeney, S.L., 2020. *Temporal and spatial variability of the open coast wave climate of Victoria, Australia*. Mar. Freshwater Res. 71 (3), 394–413. https://doi.org/10.1071/MF18489

Meucci, A., Young, I.R., Hemer, M., Trenham, C., Watterson, I.G., 2023. *140 years of global ocean wind-wave climate derived from CMIP6 ACCESS-CM2 and EC-Earth3 GCMs: Global trends, regional changes, and future projections*. J. Climate 36 (6), 1605–1631. https://doi.org/10.1175/JCLI-D-21-0929.1

Mi, J.Q., Wang, X.D., Zhai, H.K., Zhao, J.Y., Ma, C.C., He, K.P., 2025. *Improved wave direction estimation using gaussian mixture model for inertial navigation systems*. Ocean Eng. 341 (3), 122487. https://doi.org/10.1016/j.oceaneng.2025.122487

Morim, J., Hemer, M., Wang, X.L.L., Cartwright, N., Trenham, C., Semedos, A., Young, I., Bricheno, L., Camus, P., Casas-Prat, M., Erikson, L., Mentaschi, L., Mori, N., Shimura, T., Timmermans, B., Aarnes, O., Breivik, O., Behrens, A., Dobrynin, M., Menendez, M., Staneva, J., Wehner, M., Wolf, J., Kamranzad, B., Webb, A., Stopa, J., Andutta, F., 2019. *Robustness and uncertainties in global multivariate wind-wave climate projections*. Nat. Clim. Change 9 (9), 711–718. https://doi.org/10.1038/s41558-019-0542-5

Mortlock, T.R., Goodwin, I.D., McAneney, J.K., Roche, K., 2017. *The June 2016 Australian East Coast low: Importance of wave direction for coastal erosion assessment*. Water 9 (2), 121. https://doi.org/10.3390/w9020121

In press

Najafzadeh, F., Jankowski, M.Z., Giudici, A., Männikus, R., Suursaar, Ü., Viška, M., Soomere, T., 2024. *Spatiotemporal variability of wave climate in the Gulf of Riga*. Oceanologia 66 (1), 56–77. https://doi.org/10.1016/j.oceano.2023.11.001

Pereira, C., Coelho, C., 2013. *Mapping erosion risk under different scenarios of climate change for Aveiro coast, Portugal*. Nat. Hazards 69 (1), 1033–1050. https://doi.org/10.1007/s11069-013-0748-1

Rajasree, B.R., Deo, M.C., 2018. *Evaluation of estuary shoreline shift in response to climate change: A study from the central west coast of India*. Land Degrad. Dev. 29 (10), 3571–3583. https://doi.org/10.1002/ldr.3074

Rätsep, M., Parnell, K.E., Soomere, T., Kruusmaa, M., Ristolainen, A., Tuhtan, J.A., 2021. *Surface vessel localization from wake measurements using an array of pressure sensors in the littoral zone*. Ocean Eng. 233, 109156. https://doi.org/10.1016/j.oceaneng.2021.109156

Ren, H.R., Li, G.S., Cui, L.L., Zhang, Y., Ouyang, N.L., 2017. *Simulating wave climate fluctuation in the Bohai Sea related to oscillations in the East Asian circulation over a sixty year period*. J. Coast. Res. 33 (4), 829–838. https://doi.org/10.2112/JCOASTRES-D-15-00209.1

Ristolainen, A., Tuhtan, J.A., Kuusik, A., Kruusmaa, M., 2016. *Hydromast: a bioinspired flow sensor with accelerometer*. [In:] Lepora, N., Mura, A., Mangan, M., Verschure, P., Desmulliez, M. and Prescott, T. (Eds.). *Biomimetic and Biohybrid Systems. Living Machines 2016. Lecture Notes in Computer Science*, Springer, Cham, 9793, 510–517. https://doi.org/10.1007/9783319424170_55

Ristolainen, A., Tuhtan, J.A., Kruusmaa, M., 2019. *Continuous, nearbed current velocity estimation using pressure and inertial sensing*. IEEE Sens. J. 19 (24), 12398–12406. https://doi.org/10.1109/JSEN.2019.2937954

Sanuy, M., Jiménez, J.A., 2019. *Sensitivity of storm-induced hazards in a highly curvilinear coastline to changing storm directions. The Tordera delta case*. Water 11 (4), 747. https://doi.org/10.3390/w11040747

Silva, A.P., Klein, A.H.F., Fetter, A.F.H., Hein, C.J., Méndez, F.J., Broggio, M.F., Dalinghaus, C., 2020. *Climate-induced variability in South Atlantic wave direction over the past three millennia*. Sci. Rep.-UK 10 (1), 1855. https://doi.org/10.1038/s41598-020-75265-5

Skudra, M., Lips, U., 2017. *Characteristics and inter-annual changes in temperature, salinity and density distribution in the Gulf of Riga*. Oceanologia 59 (1), 37–48. https://doi.org/10.1016/j.oceano.2016.07.004

Sokolov, A., Chubarenko, B., 2024. *Baltic Sea wave climate in 1979–2018: Numerical modelling results*. Ocean Eng. 297, 117088. https://doi.org/10.1016/j.oceaneng.2024.117088

Soomere, T., 2003. *Anisotropy of wind and wave regimes in the Baltic Proper*. J. Sea Res. 49 (4), 305–316. https://doi.org/10.1016/S1385-1101(03)00034-0

Soomere, T., Bishop, S.R., Viška, M., Räämet, A., 2015. *An abrupt change in winds that may radically affect the coasts and deep sections of the Baltic Sea*. Clim. Res. 62 (2), 163–171. https://doi.org/10.3354/cr01269

Soomere, T., Jankowski, M.Z., Eelsalu, M., Parnell, K.E., Viška, M., 2025. *Alongshore sediment transport analysis for a semi-enclosed basin: a case study of the Gulf of Riga, the Baltic Sea*. Ocean Sci. 21 (2), 619–641. https://doi.org/10.5194/os-21-619-2025

Soomere, T., Keevallik, S., 2001. *Anisotropy of moderate and strong winds in the Baltic Proper*. Proc. Est. Acad. Sci. Eng. 7 (1), 35–49. https://doi.org/10.3176/eng.2001.1.04

Soomere, T., Männikus, R., Pindsoo, K., Kudryavtseva, N., Eelsalu, M., 2017. *Modification of closure depths by synchronisation of severe seas and high water levels*. Geo-Mar. Lett. 37 (1), 35–46. https://doi.org/10.1007/s00367-016-0471-5

Soomere, T., Pindsoo, K., Bishop, S.R., Käärd, A., Valdmann, A., 2013. *Mapping wave set-up near a complex geometric urban coastline*. Nat. Hazard. Earth Sys. 13 (11), 3049–3061. https://doi.org/10.5194/nhess-13-3049-2013

Soomere, T., Viška, M., 2014. *Simulated sediment transport along the eastern coast of the Baltic Sea*. J. Marine Syst. 129, 96–105. https://doi.org/10.1016/j.jmarsys.2013.02.001

Stevens, A.W., Ruggiero, P., Parker, K.A., Vitousek, S., Gelfenbaum, G., Kaminsky, G.M., 2024. *Climate controls on longshore sediment transport and coastal morphology adjacent to engineered inlets*. Coast. Eng. 194, 104617. https://doi.org/10.1016/j.coastaleng.2024.104617

Stiebrins, O., Väling, P., 1996. *Bottom sediments of the Gulf of Riga*. Geological Survey of Latvia, 4 pp.

Su, M.-Y., Green, A.W., 1984. *Coupled two- and three-dimensional instabilities of surface gravity waves*. Phys. Fluids 27 (11), 2595–2597. https://doi.org/10.1063/1.864556

Timmermans, B.W., Gommenginger, C.P., Dodet, G., Bidlot, J.-R., 2020. *Global wave height trends and variability from new multimission satellite altimeter products, reanalyses, and wave buoys*. Geophys. Res. Lett. 47, e2019GL086880. https://doi.org/10.1029/2019GL086880

Thomas, T., Phillips, M.R., Williams, A.T., Jenkins, R.E., 2011. *Short-term beach rotation, wave climate and the North Atlantic Oscillation (NAO)*. Progr. Phys. Geogr. 35 (3), 333–352. https://doi.org/10.1177/03091333103974

Tsyrulnikov, A., Tuuling, I., Hang, T., 2008. *Streamlined topographical features in and around the Gulf of Riga*

In Press

as evidence of Late Weichselian glacial dynamics. Geol. Q. 52, 81–89.

Ulsts, V., 1998. *Latvian coastal zone of the Baltic Sea*. Atlas. State Geological Survey of Latvia.

USACE, 2002. *Coastal Engineering Manual*. Manual No. 1110-2-1100. Department of the Army, US Army Corps of Engineers. https://www.publications.usace.army.mil/USACE-Publications/Engineer-Manuals/u43544q/636F617374616C20656E67696E656572696E67206D616E75616C/ (last access: 16 January 2025)

Wiggins, M., Scott, T., Masselink, G., Russell, P., McCarroll, R.J., 2019. *Coastal embayment rotation: Response to extreme events and climate control, using full embayment surveys*. Geomorphology 327, 385–403. https://doi.org/10.1016/j.geomorph.2018.11.014

Wiguna, T., Dompeipen, A.C., 2025. *Historical analysis of ocean climate hazard indicators and sea level projection in the Karawang region, Indonesia*. B. Geophys. Oceanogr. 66 (3), 331–350. https://doi.org/10.4430/bgo00497

Woo, H.J., Park, K.A., Jeong, K.Y., Byun, D.S., Oh, H.J., 2023. *Spatial and temporal variability of significant wave height and wave direction in the Yellow Sea and East China Sea*. J. Korean Earth Sci. Soc. 44 (1), 1–12. https://doi.org/10.5467/JKESS.2023.44.1.1

Xu, W., Chen, S.L., Ji, H.Y., Hu, T.H., Zhong, X.J., Li, P., 2024. *Dynamics of sandy shorelines and their response to wave climate change in the east of Hainan Island, China*. J. Mar. Sci. Eng. 12 (11), 1921. https://doi.org/10.3390/jmse12111921

Young, I.R., Ribal, A., 2019. *Multiplatform evaluation of global trends in wind speed and wave height*. Science 364, 548–552. https://doi.org/10.1126/science.aav9527

Young, I.R., Zieger, S., Babanin, A.V., 2011. *Global trends in wind speed and wave height*. Science 332 (6028), 451–455. https://doi.org/10.1126/science.1197219

Zacharioudaki, A., Reeve, D.E., 2011. *Shoreline evolution under climate change wave scenarios*. Climatic Change 108 (1–2), 73–105. https://doi.org/10.1007/s10584-010-0011-7

in press